

# Study of 6.5 kV injection enhanced floating emitter (IEFE) IGBT switching behavior and its improved short-circuit robustness

<sup>1</sup>Madhu-Lakshman Mysore, <sup>1</sup>Thomas Basler, <sup>1</sup>Josef Lutz, <sup>2</sup>Roman Baburske, <sup>2</sup>Hans-Joachim Schulze, <sup>2</sup>Franz-Josef Niedernostheide

<sup>1</sup>Chemnitz University of Technology, Chair of Power Electronics, Chemnitz, Germany,  
Tel: +49 371/531-36091

<sup>2</sup>Infineon Technologies AG, Neubiberg, Germany

## Abstract

*In this work the improved short-circuit robustness of a new IGBT along with its switching behavior is investigated. The application of the recently proposed injection enhanced floating emitter (IEFE) concept to a 6.5 kV IGBT results in a higher hole current injection from the buried floating p-islands in front of the p-collector under short-circuit conditions. Hence, this concept provides a significantly improved short-circuit robustness compared to IGBT without p-islands and for the same design. The simulated results of the IEFE IGBTs depict the suppression of electrical current crowding at the collector-side without affecting the static and dynamic losses of the device.*

**Keywords:** IGBT, short-circuit, current filaments, switching behavior, TCAD simulation.

## INTRODUCTION

IGBTs are frequently used power semiconductor switches in the field of power electronics in a wide range of applications. One of the superior features of IGBTs is the ability to withstand both a high voltage and high current under short-circuit (SC) conditions for a certain time interval. The short-circuit safe operating area (SC-SOA) limit was investigated by many authors for IGBTs of different voltage classes from 1200 V to 6500 V [1-6]. The results in ref. [1,2,6] explain that the IGBT short-circuit destruction can be caused by the formation of current filaments at the collector side. In the experimental investigations, non-destructive current filaments in IGBTs operating under SC conditions were observed by using thermo-reflectance microscopy (TRM) [7]. In the experimental investigations, these current destructions occur far beyond the safe operating area (SOA) of the IGBT.

A new IEFE IGBT structure, which suppresses the formation of current filamentation at the collector side and offers improved SC robustness has been demonstrated for the 1200 V class with simplified IGBT structure by TCAD simulation [8].

The critical SC current for a conventional IGBT can be increased by increasing the p-emitter doping. But the increase in the p-emitter doping leads to an increase in the leakage current during static blocking and reduces the thermal robustness of the IGBT. Hence, the new IEFE IGBT with p-islands has been investigated for an improved SC robustness without compromising the thermal robustness of the IGBT and the dynamic losses

of the device. In this work, a realistic front-side trench-gate 6.5 kV IGBT structure has been designed, and device simulations were carried out with Sentaurus TCAD. The static characteristics of the IEFE IGBT have been compared with a reference IGBT model along with the switching behavior to study the  $E_{off}$ - $V_{CE,sat}$  trade-off relationship. The switching behavior of the new IGBT structure has been investigated in detail at different parasitic inductances and for different nominal currents. Also, SC simulations have been performed on 6.5 kV IEFE IGBTs to demonstrate the improved SC capability in comparison to the reference IGBT structure.

## IGBT STRUCTURES

Fig. 1(a) shows a reference trench-gate 6.5 kV IGBT structure with uniform field stop (FS) at the collector side. In the IEFE IGBT structure, the floating p-islands are implemented inside the field-stop area and in front of the p-emitter at the anode-side to amplify the hole injection from the backside as shown in Fig. 1(b). The reference IGBT and the IEFE IGBT structures have a similar front-side design, base doping, and field-stop profile.

The design and placement of the floating p-islands are optimized in such a way that the static and dynamic behavior of the IEFE IGBT is comparable to the reference IGBT. The floating p-amplification stage design and placement is kept constant throughout this paper and the simulation results are compared with reference IGBTs. For the IEFE structure, the doping of

the  $p$ -amplification stage is  $1e18 \text{ cm}^{-3}$  and the  $p$ -emitter is doped with  $1e17 \text{ cm}^{-3}$  as mentioned in [8]. These  $p$ -islands cover a certain lateral area at the collector-side and are separated from the  $p$ -emitter by an  $n$ -barrier layer. The  $n$ -barrier layer resistivity is selected in such a way that the electric field should not influence the breakdown voltage during static forward blocking of the IGBT.

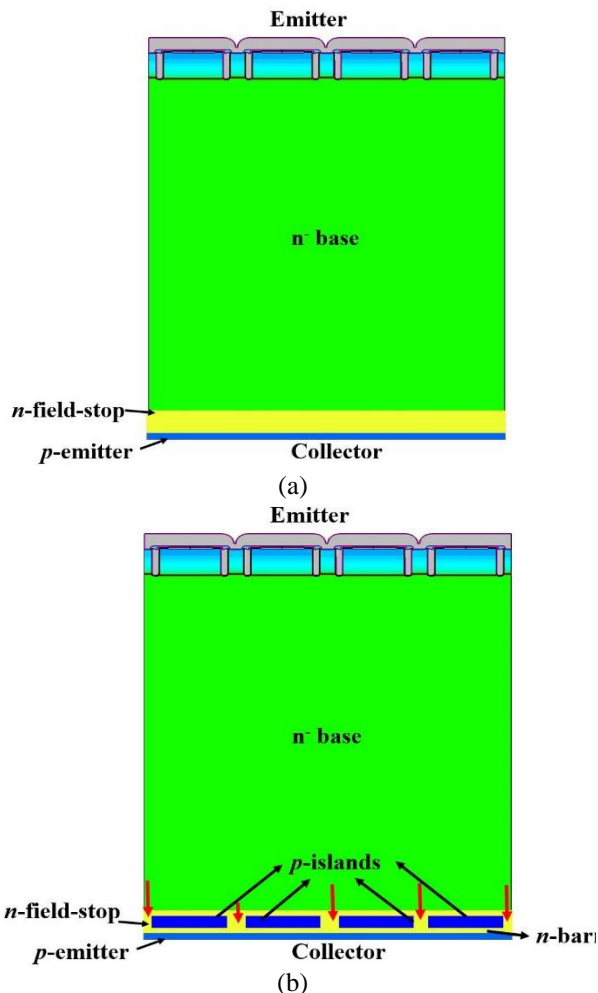


**Fig. 1:** Real front-side trench-gate 6.5 kV IGBT (a) reference structure without  $p$ -islands in front of the  $p$ -emitter, (b) IEFEB IGBT structure with  $p$ -islands in front of the  $p$ -emitter.

The IEFEB IGBT physics can be explained by means of the bipolar current gain ( $\alpha_{\text{pnp}}$ ) of the  $\text{pnp}$ -transistor in the IGBT. The  $\alpha_{\text{pnp}}$  is a product of emitter injection efficiency ( $\gamma$ ) and the transport factor ( $\alpha_{\text{T}}$ ). The control of  $\alpha_{\text{pnp}}$  is strongly dependent on the emitter efficiency of the IGBT [9]. The ratio of the hole current density ( $j_{\text{p}}$ ) to the total current density ( $j$ ) at the collector side is defined as the emitter efficiency.

Hence, an enhanced hole density at the collector side due to the  $p$ -islands will lead to higher bipolar current gain for the IEFEB structure in comparison to the reference IGBT. Thus, the critical field bending at the collector-side of the IGBT is more efficiently suppressed. Additionally, the IEFEB IGBT shows two different emitter

efficiencies at the collector-side. A more detailed IEFEB IGBT physics explanation can be found in [8].

## STATIC-CHARACTERISTICS - DEVICE SIMULATION

In this section, for the designed 6.5 kV IGBT structures, initially static characteristic simulations are described. The simulated IGBT structures have a rated current of 30 A. For these simulations, the Phillip's unified mobility model, University of Bologna avalanche model, Shockley-Read-Hall (SRH) and Auger recombination models and the Slotboom model for effective intrinsic density were utilized. The static characteristic simulations were isothermal. For the electro-thermal switching and SC simulations, self-heating was considered with a thermal boundary condition at the collector contact and a thermal resistance of 0.57 K/W.

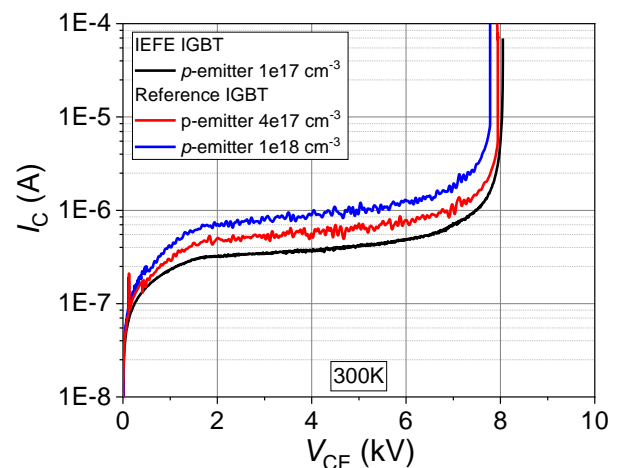


**Fig. 2:** Leakage current behavior for two different  $p$ -emitter doping concentrations in the reference IGBT structure (red and blue lines) and the IEFEB IGBT (black) at 300 K.

The leakage current behavior during static blocking at 300 K is compared for the reference IGBT and the IEFEB IGBT in Fig. 2. The increased leakage current and the decreased blocking voltage are clearly seen in the reference IGBT as the  $p$ -emitter doping is increased. However, the IEFEB structure shows a slightly reduced leakage current and similar blocking voltage compared to the reference IGBT with  $p$ -emitter doping of  $4e17 \text{ cm}^{-3}$ .

During the blocking state, the IEFEB IGBT shows a smaller leakage current even though the  $p$ -islands have a doping concentration of  $1e18 \text{ cm}^{-3}$ . The electric field is much lower across the  $p$ -islands in comparison to the emitter-side during blocking mode and the  $p$ -islands are embedded in the field-stop region. During the forward blocking state, the leakage current flows through the gap between the  $p$ -islands marked by red arrows in Fig. 1(b). Thus, the influence of the  $p$ -islands during the static blocking can be neglected.

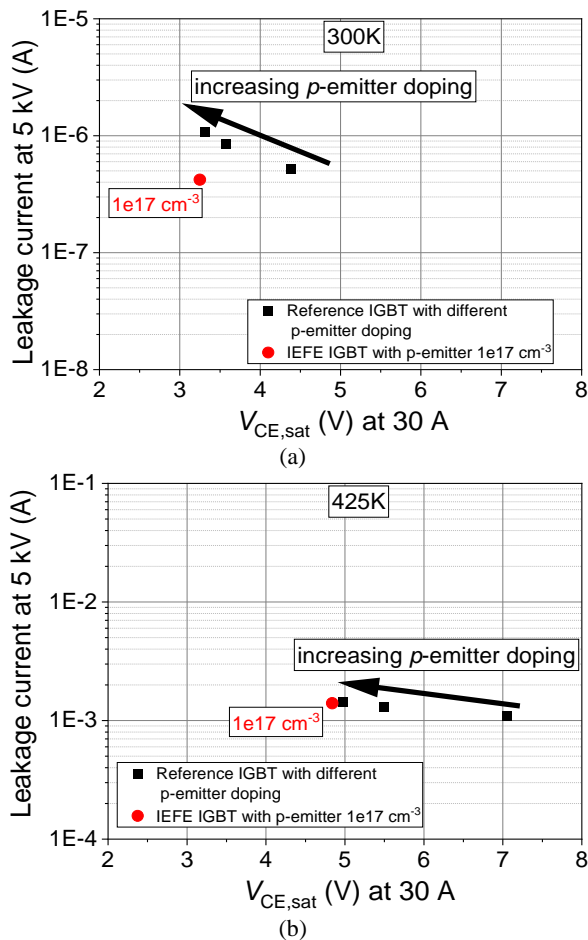


**Fig. 3:** Comparison of the leakage current at 5 kV as a function of  $V_{CE,sat}$  between the reference IGBT with different  $p$ -emitter doping and the IEFEBT with  $p$ -emitter doping  $1e17 \text{ cm}^{-2}$  (a) 300 K (b) 425 K.

In Fig. 3, the leakage current has been plotted as a function of  $V_{CE,sat}$  for the reference IGBTs with different  $p$ -emitter doping and the IEFEBT at 300 K and 425 K. For the reference IGBT structure, as the  $p$ -emitter doping increases, the increase in leakage current is more prominent at 300 K in comparison to 425 K. For the total leakage current at 425 K, the diffusion leakage current contribution is much higher than the space-charge region leakage current.

The  $V_{CE,sat}$  of the reference IGBT strongly reduces with an increase in the  $p$ -emitter doping as the hole injection increases strongly from the collector-side and therefore the bipolar current gain of the IGBT increases accordingly. Even though the  $p$ -emitter doping of the IEFEBT structure is  $1e17 \text{ cm}^{-3}$ , the  $V_{CE,sat}$  of the IEFEBT structure is comparable to that of reference IGBT with the highest  $p$ -emitter doping at 300 K and 425 K.

The IEFEBT structure with highly doped  $p$ -islands – located in the field-stop layer in front of the  $p$ -collector doping and separated by an  $n$ -barrier layer – offers an opportunity to reduce the collector-side  $p$ -emitter doping. Therefore, it is possible to attain a slightly lower leakage current [8].

## DYNAMIC SWITCHING BEHAVIOR

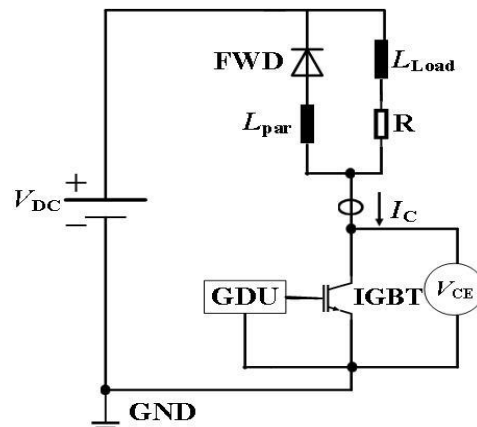


**Fig. 4:** Circuit for turn-off simulations.

A double-pulse setup with inductive load is used for the dynamic switching simulation (Fig. 4). The simulated IGBT can be controlled by the gate driver unit (GDU). The circuit consists of a parasitic inductance ( $L_{par}$ ), a load inductance ( $L_{Load}$ ), and a freewheeling diode (FWD).

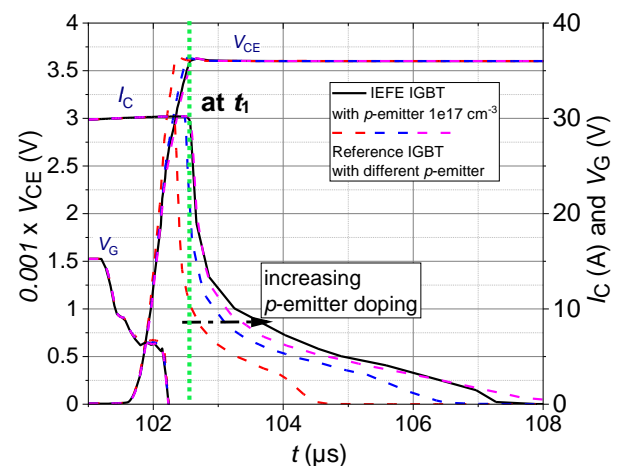


**Fig. 5:** Comparison of the turn-off behavior between the reference IGBT with different  $p$ -emitter doping concentrations and the IEFEBT. Simulation conditions:  $V_{DC} = 3600 \text{ V}$ ,  $I_C = 30 \text{ A}$ ,  $L_{Load} = 12 \text{ mH}$ ,  $V_{GE} = -15 \text{ V}/+15 \text{ V}$ ,  $L_{Load} = 12 \text{ mH}$ ,  $L_{par} = 250 \text{ nH}$ ,  $R_{G,ON} = 2 \Omega$ ,  $R_{G,OFF} = 10 \Omega$ ,  $t_{pulse} = 100 \mu\text{s}$ ,  $T_{start} = 425 \text{ K}$ .

The simulated turn-off behavior of the reference IGBT with different  $p$ -emitter doping and the IEFEBT are compared at 425 K in Fig. 5. The turn-off simulations are carried out using a circuit as shown in Fig. 4. For turn-off simulations, the collector current is turned off at a rated current of the IGBT by switching the  $V_{GE}$  from +15 V to -15 V. As the IGBT is turned off, the voltage increases to the applied DC-link voltage  $V_{DC}$  of 3600 V across the IGBT with a turn-off peak slightly higher than  $V_{DC}$  due to  $L_{par}$  in the circuit. The considered parasitic inductance of 250 nH is very small for a single chip, and hence a very small overvoltage is seen in Fig. 5. As the  $p$ -emitter doping increases for the reference IGBTs, the tail current in the IGBTs increases and  $dV_{CE}/dt$  decreases slightly.

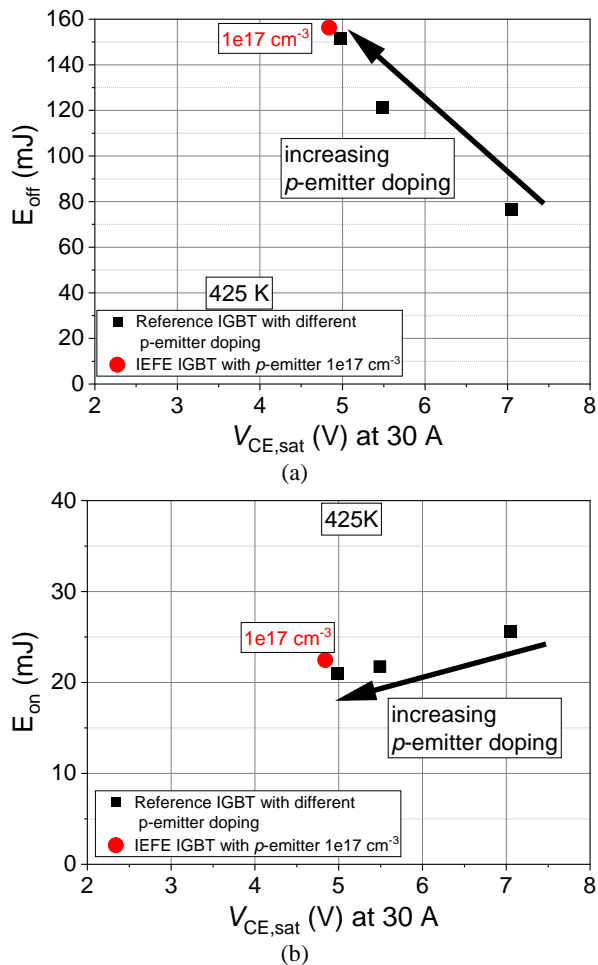


**Fig. 6:** Comparison of (a) turn-off losses (b) turn-on losses as a function of  $V_{CE,sat}$  between the reference IGBT with different  $p$ -emitter doping concentrations and the IEFEB IGBT using the same FWD. Simulation conditions:  $V_{DC} = 3600 \text{ V}$ ,  $V_{GE} = -15/+15 \text{ V}$ ,  $I_C = 30 \text{ A}$ ,  $L_{Load} = 12 \text{ mH}$ ,  $L_{par} = 250 \text{ nH}$ ,  $R_{G,ON} = 2 \Omega$ ,  $R_{G,OFF} = 10 \Omega$ ,  $t_{pulse} = 100 \mu\text{s}$ ,  $T_{start} = 425 \text{ K}$ .

The turn-off behavior of the IEFEB IGBT is comparable with the reference IGBT with the highest  $p$ -emitter doping as shown in Fig. 5.

For the simulated switching behavior at 425 K, the turn-off and turn-on losses are plotted as a function of  $V_{CE,sat}$  for the IEFEB IGBT and the reference IGBTs in Fig. 6. The IEFEB IGBT shows slightly lower  $V_{CE,sat}$  and moderately higher  $E_{off}$  losses compared to the reference IGBT with the highest  $p$ -emitter doping. However, the IEFEB IGBT is on the same  $E_{off} - V_{CE,sat}$  trade-off curve as the reference IGBT. The  $E_{on}$  losses of the IEFEB IGBT are slightly higher in comparison to the reference IGBT with different  $p$ -emitter doping.

The electric field and charge carrier densities of the IEFEB IGBT and the reference IGBT with the highest  $p$ -emitter doping are compared in Fig. 7 at time point  $t_1$  from Fig. 5. The distributions of the electric field and the carrier densities are approximately the same for both simulated devices. This is valid in the plasma and the space-charge region.

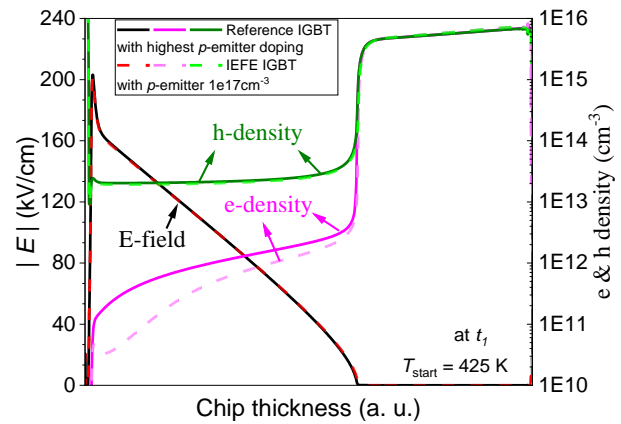


**Fig. 7:** Comparison of electric field and charge carrier densities between the reference IGBT with highest  $p$ -emitter doping and the IEFEB IGBT at time point  $t_1$  in Fig. 5 (green dotted line).

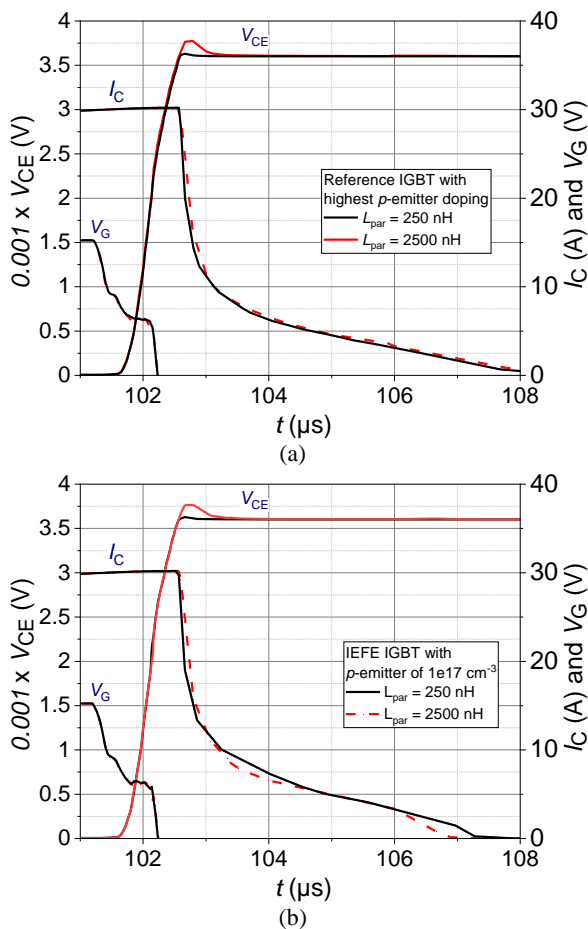
## DYNAMIC SWITCHING BEHAVIOR UNDER HIGHER PARASITIC INDUCTANCES

One of the important parameters under switching is the parasitic inductance ( $L_{par}$ ). Further turn-off simulations are performed for the reference IGBT and the IEFEB IGBT with approximately similar  $E_{off}$  losses at two different parasitic inductances as shown in Fig. 8. Both IGBTs show a higher turn-off  $V_{CE}$  peak at higher parasitic inductance. The  $dV_{CE}/dt$  remains approximately the same even at higher  $L_{par}$  for both IGBTs. The IEFEB and the reference structure turn-off tail current behavior is approximately comparable to  $L_{par} = 250 \text{ nH}$  even if the  $L_{par}$  is increased by 10 times.

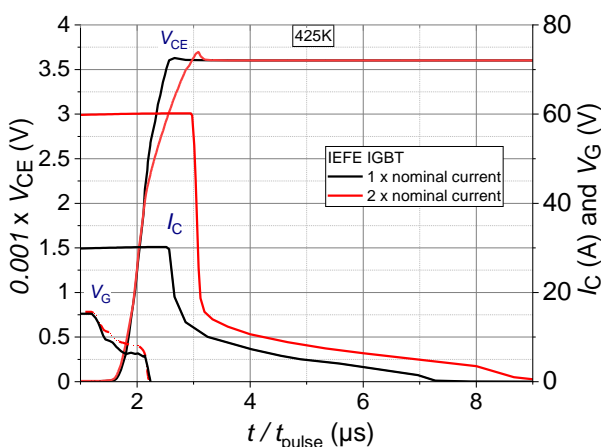
As displayed in Fig. 9, the turn-off behavior of the IEFEB IGBT is compared at two different nominal currents at 425 K. The IEFEB structure shows a longer tail current at 60 A compared to the rated current. At a higher nominal current, the IEFEB IGBT shows a higher turn-off  $V_{CE}$  peak and lower  $dV_{CE}/dt$  after 2 kV in comparison to 30 A. The IEFEB structure does not show any undesirable behavior at two times the rated current.

## ELECTRO-THERMAL SC SIMULATIONS

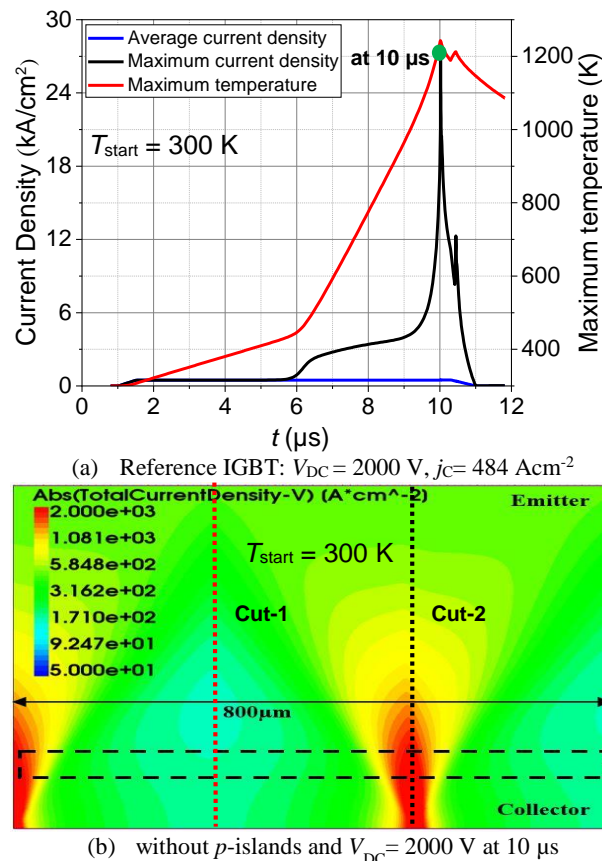
In this section, electro-thermal SC device simulations are performed with a wider structure of  $800 \mu\text{m}$  using a simplified front-side IGBT structure to reduce the simulation time [6]. Also, a wider structure of  $800 \mu\text{m}$  makes possible to investigate the behavior of current filamentation. In order to study the enhanced SC capability of the IEFEB IGBTs, the bipolar current gain of the simplified front-side IGBT structure was worsened for both the reference and IEFEB IGBT structures. A simple time-dependent SC current pulse was simulated with a 300 K initial temperature ( $T_{start}$ ) and with a constant DC-link voltage.



**Fig. 8:** Comparison of the turn-off behavior at different parasitic inductances of (a) the reference IGBT with highest  $p$ -emitter doping and of (b) the IEFEB IGBT. Simulation conditions:  $V_{DC} = 3600$  V,  $V_{GE} = -15/+15$  V,  $I_C = 30$  A,  $L_{Load} = 12$  mH,  $R_{G,ON} = 2$   $\Omega$ ,  $R_{G,OFF} = 10$   $\Omega$ ,  $t_{pulse} = 100$   $\mu$ s,  $T_{start} = 425$  K.

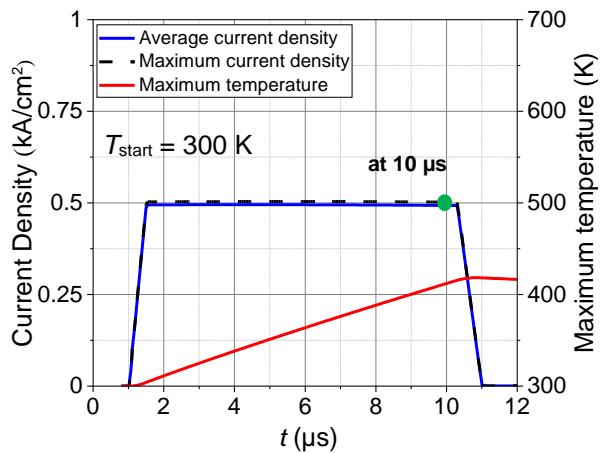
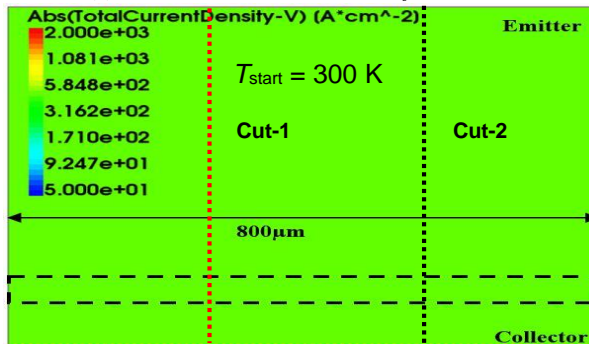


**Fig. 9:** Comparison of turn-off behavior at different nominal current for the IEFEB IGBT. Simulation conditions:  $V_{CE} = 3600$  V,  $V_{GE} = -15/+15$  V,  $L_{Load} = 12$  mH,  $L_{par} = 250$  nH,  $R_{G,ON} = 2$   $\Omega$ ,  $R_{G,OFF} = 10$   $\Omega$ ,  $T_{start} = 425$  K.



**Fig. 10:** (a) Transients of the average current density, maximum current density and maximum temperature under given SC conditions for a 6.5 kV reference IGBT (b) absolute total current density distribution at 10  $\mu$ s.

Fig. 10 shows the transients of the average and maximum current densities and the time-dependent behavior of the maximum temperature during the SC event at  $V_{DC} = 2000$  V,  $j_C = 484$  Acm<sup>-2</sup>,  $T_{start} = 300$  K and SC pulse length ( $t_{sc}$ ) of 10  $\mu$ s for the reference IGBT. The rise time and fall time were set to 1  $\mu$ s. The bottom picture in Fig. 10 shows the absolute value of the total current density distribution in IGBTs at the beginning of the SC turn-off process (10  $\mu$ s) for the reference IGBTs. The average and maximum current densities were extracted from a window shown in the black dashed box in Fig. 10(b). The maximum temperature was extracted from the whole silicon region. At 5.8  $\mu$ s, the average and maximum current density curves start to split in the reference IGBT. The current flow becomes more inhomogeneous throughout the structure. The slope of the maximum temperature transient increases rapidly after 6.0  $\mu$ s and reaches a value of 1260 K at 10  $\mu$ s inside the current filament of cut 2. At time point 10  $\mu$ s, the IGBT device shows one and a half current filaments. The maximum current density is about 26 kA/cm<sup>2</sup> higher than the average current density. The simulated edge-to-edge filament lateral spacing is more than 450  $\mu$ m. There is a correlation between the lateral distance between the current filaments and the width of the quasi-plasma region and the relationship between the width of the current filament and the width of the high-field region [10].

(a) IEFE IGBT:  $V_{DC} = 2000$  V,  $j_C = 484$  Acm<sup>-2</sup>(b) with  $p$ -islands and  $V_{DC} = 2000$  V at  $10 \mu\text{s}$ 

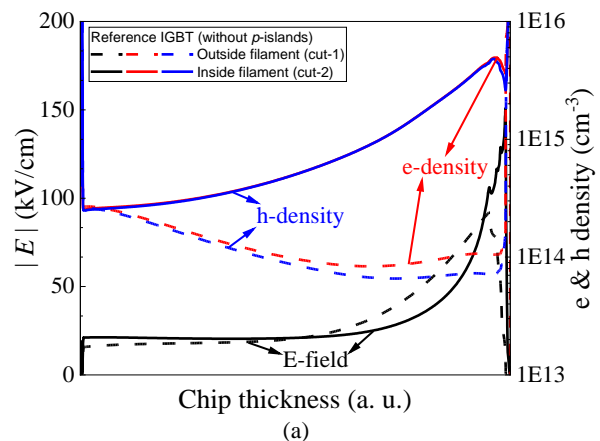
**Fig. 11:** (a) Transients of the average current density, maximum current density and maximum temperature under given SC conditions for a 6.5 kV IEFE IGBT (b) absolute total current density distribution at  $10 \mu\text{s}$ .

Fig. 11 depicts the transients of the average and maximum current densities and the transient of the maximum temperature during the SC event for the IEFE IGBT with SC conditions of  $V_{DC} = 2000$  V,  $j_C = 484$  Acm<sup>-2</sup>,  $T_{start} = 300$  K and SC pulse length ( $t_{SC}$ ) of  $10 \mu\text{s}$ . There is no split in the average and maximum current density curve [Fig. 11(a)] for the same SC conditions as for the reference. The average and maximum current densities were extracted from a window shown in the black dashed box in Fig. 11(b). The maximum temperature for the IEFE structure is 425 K at  $10 \mu\text{s}$ , which is 835 K less than the reference structure with similar SC conditions. Also, the current distribution in the IEFE IGBT is homogenous in lateral direction in Fig. 11(b).

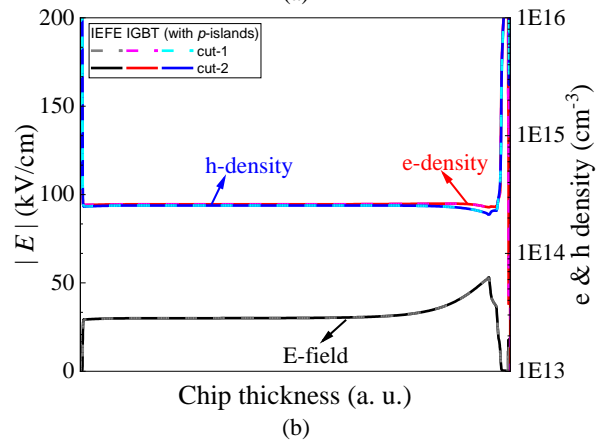
Fig. 12 shows a vertical cross-section of the absolute value of the electric-field strength, electron density and hole density in the reference and IEFE IGBT structures at  $10 \mu\text{s}$  from two different cuts in Fig. 10(b) and Fig. 11(b) respectively.

For the reference IGBT, the shift of the electric field peak to the  $n$ -base/ $n$ -field-stop junction is due to the higher number of electrons than the number of holes at the collector-side of the base region. Due to the strong current filaments at  $10 \mu\text{s}$ , the concentration of the quasi-plasma in the reference IGBT is higher inside the current

filament than outside the filament [Fig. 12(a)]. The carrier concentration inside the current filament is roughly 50 times larger than outside the filament. There is an increase in the peak electric field at the filament positions. However, the current distribution for the structure with  $p$ -islands is uniform [Fig. 11(b)]. The electric-field of the IEFE IGBT at the collector-side is three times smaller in comparison to the reference IGBT (Fig. 12). Also, the electric field strength, electron and hole densities show a homogeneous lateral distribution in the device and overlap on each other for both cuts [Fig. 12(b)]. The main reason is the stronger hole injection from the back-side which partly compensates the negative charges in the front of the  $p$ -emitter.



(a)



(b)

**Fig. 12:** Absolute value of the electric-field strength, electron and hole density distribution in IGBTs during SC at  $V_{DC} = 2000$  V,  $j_C = 484$  Acm<sup>-2</sup>,  $T_{int} = 300$  K at  $10 \mu\text{s}$  (a) reference IGBT (b) IEFE IGBT. For the cuts ref. to Fig. 10 and Fig. 11.

## SC FILAMENTATION CRITERION

In order to estimate the short-circuit current which provokes strong filamentation and early destruction in the 6.5 kV reference and the IEFE IGBT, a simple simulation procedure is used from [2]. A transfer characteristic of 6.5 kV IGBT structure is simulated for a particular  $V_{CE}$ . During the  $V_{GE}$  ramp, the ratio in Eq. (1) is considered [11].

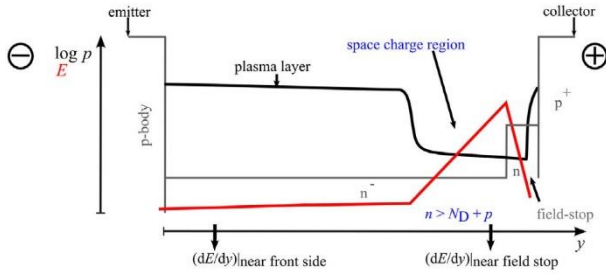


**Fig. 13:** Schematic representation of the hole density (black) and the electric-field strength (red) during the SC event in IGBT at high current [2].

$$c \approx \frac{(dE/dy)|_{\text{near field stop}}}{(dE/dy)|_{\text{near front side}}} = 2 \quad (1)$$

where  $(dE/dy)|_{\text{near field stop}}$  is the field gradient close to the field-stop junction and  $(dE/dy)|_{\text{near front side}}$  represents the field gradient close to the emitter-side MOS structure of a short-circuit operation point. If the ratio of the two slopes is close to 1, the whole base region is covered with the space-charge region. Hence, there is no quasi-plasma layer and thus it is an uncritical condition. However, when  $c$  is higher than 1, the formation of current filaments is possible due to the bigger quasi-plasma layer [11].

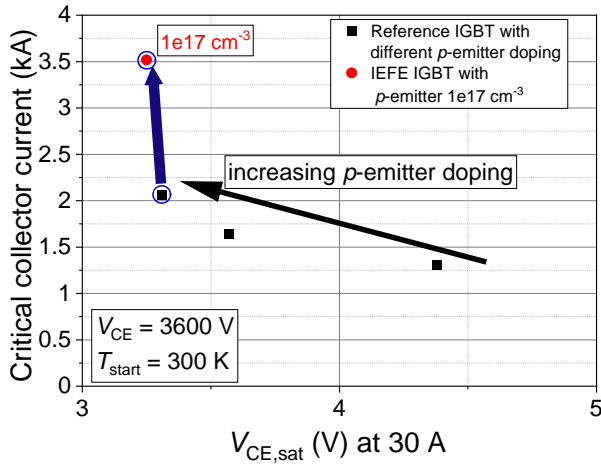


**Fig. 14:** Comparison of the critical collector current as a function  $V_{CE,sat}$  between the reference IGBT with different  $p$ -emitter doping and the IEFEB IGBT with  $p$ -emitter doping of  $1e17 \text{ cm}^{-3}$  at 3600 V and  $T_{start} = 300 \text{ K}$ .

The simulated SC robustness of the reference 6.5 kV IGBT with different  $p$ -emitter doping is compared with the IEFEB IGBT in Fig. 14 for a DC-link voltage of 3600V and at 300 K. The criterion from Eq. (1) is used to determine the formation of a current filament. The IEFEB structure shows an improved SC robustness of 1.7 times the value of the reference IGBT with comparable  $V_{CE,sat}$ . Here, the leakage current of the IEFEB structure is slightly lower in comparison to the reference IGBT with approximately similar  $V_{CE,sat}$ .

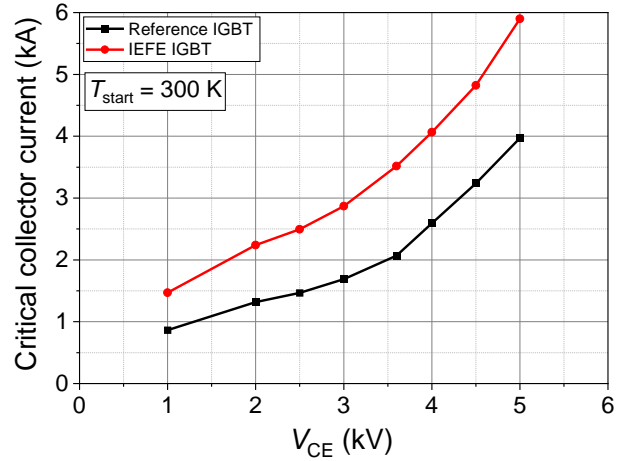


**Fig. 15:** Comparison of the critical collector current as a function of  $V_{CE}$  between the reference IGBT and the IEFEB IGBT for approximately similar  $V_{CE,sat}$ . See Fig. 14 for the considered circle points.

The simulated critical collector current is plotted as a function of high  $V_{CE}$  for the reference IGBT and the IEFEB IGBT with approximately similar  $V_{CE,sat}$  in Fig. 15. As  $V_{CE}$  increases, the critical collector current increases. The IEFEB structure exhibits higher SC robustness in comparison to the reference 6.5 kV IGBT due to the suppression of the current filaments. For both the simulated IGBT structures, the critical collector current at 1000 V and 2000 V could be much higher than the plotted values in Fig. 15. From the simple criterion used here, Eq. (1), the critical current is determined as soon as  $c$  reaches a value of 2. But due to the existence of non-destructive current filaments at 1000 V and 2000 V, the value of  $c$  shall be much higher than 2 [11]. Hence, the SC robustness can be expected to be much higher at 1000 V and 2000 V DC-link for both IGBTs [11].

## CONCLUSION

The  $V_{CE,sat}$  of the IEFEB IGBT and the reference IGBT with highest  $p$ -emitter doping are comparable. The new IGBT structure shows a lower leakage current and the higher forward blocking voltage in comparison to the reference IGBT. The switching behavior is similar. Both IGBTs are on the same  $E_{off} - V_{CE,sat}$  trade-off. Even for 10 times higher parasitic inductance and two times nominal current, the IEFEB and reference structure does not show an undesired behavior during switching simulations. The SC capability of the 6.5 kV IEFEB IGBT has been improved significantly, because the formation of the current crowding during SC can be suppressed to a high extent. This higher SC robustness is achieved without compromising the static and dynamic performance of the IGBT device.

## REFERENCES

- [1] A. Kopta, M. Rahimo, U. Schlapbach, et al., "Limitation of the Short-Circuit Ruggedness of High Voltage IGBTs," in Proc. ISPSD, 2009, pp. 33-36.
- [2] R. Baburske, V. Treck, F. Pfirsch, F. J. Niedernostheide, et al., "Comparison of Critical Current Filaments in IGBT Short Circuit and during Diode Turn-off," in Proc. ISPSD, 2014, pp. 47-50.
- [3] H. Hagino, J. Yamashita, A. Uenishi, et al., "Avalanche Characteristics and Failure Mechanism of High Voltage Diodes," IEEE Transactions on Electron Devices, Vol. ED-13, No. 11, pp. 754-758, 1996
- [4] M. Tanaka, A. Nakagawa, "Simulation studies for Avalanche induced short-circuit current crowding of MOSFET-Mode IGBT," in Proc. ISPSD, 2015, pp. 121-124.
- [5] M. Tanaka, A. Nakagawa, "Growth of short-circuit current filament in MOSFET-Mode IGBTs," in Proc. ISPSD, 2016, pp. 319-322.
- [6] R. Bhojani, S. Palanisamy, R. Baburske, et al., "Simulation study on collector side filament formation at short-circuit in IGBTs," in Proc. of ISPS, Prague, 2016, pp. 70-76.
- [7] R. Bhojani, J. Kowalsky, J. Lutz, D. Kendig, R. Baburske, H. J. Schulze, F. J. Niedernostheide, "Observation of Current Filaments in IGBTs with Thermo-Reflectance Microscopy," in Proc. ISPSD, May 2018, pp. 164-167.
- [8] R. Bhojani, J. Lutz, R. Baburske et al., "A Novel Injection Enhanced Floating Emitter (IEFE) IGBT Structure Improving the Ruggedness against Short-Circuit and Thermal Destruction," in Proc. of ISPSD, May 2017, pp. 113-116.
- [9] J. Lutz, H. Schlangenotto, et al, Semiconductor Power Devices-Physics, Characteristic, Reliability. Springer, Second edition, 2018.
- [10] R. Bhojani, M-L. Mysore, R. Raihan et al, "Current Filament Behavior in Different Voltage Class IGBTs using Measurements and Simulations," in Proc. ISPSD, Sep. 2020, pp. 446-449.
- [11] R. Baburske, F. J. Niedernostheide, H.-J. Schulze, et al, "Unified view on energy and electrical failure of the short-circuit operation of IGBTs," Microelectronics Reliability, 2018, Vol. 88-90, pp. 236-241.

## Addresses of the authors

Madhu-Lakshman Mysore, Reichenhainer Str. 70, Chemnitz, Germany, madhu-lakshman.mysore@etit.tu-chemnitz.de

Thomas Basler, Reichenhainer Str. 70, Chemnitz, Germany, thomas.basler@etit.tu-chemnitz.de

Josef Lutz, Reichenhainer Str. 70, Chemnitz, Germany, josef.lutz@etit.tu-chemnitz.de

Roman Baburske, Infineon Technologies AG, Neubiberg, Germany, roman.baburske@infineon.com

Hans-Joachim Schulze, Infineon Technologies AG, Neubiberg, Germany, schulze.external9@infineon.com

Franz-Josef Niedernostheide, Infineon Technologies AG, Neubiberg, Germany, franz-josef.niedernostheide@infineon.com